Orientation dependence of broadband acoustic backscattering from live squid

Wu-Jung Lee, Andone C. Lavery, and Timothy K. Stanton
Department of Applied Ocean Physics and Engineering, Woods Hole Oceanographic Institution, Woods Hole, Massachusetts 02543

(Received 1 April 2011; revised 7 November 2011; accepted 19 March 2012)

A controlled laboratory experiment of broadband acoustic backscattering from live squid (*Loligo pealeii*) was conducted using linear chirp signals (60–103 kHz) with data collected over the full 360° of orientation in the lateral plane, in <1° increments. The acoustic measurements were compared with an analytical prolate spheroid model and a three-dimensional numerical model with randomized squid shape, both based on the distorted-wave Born approximation formulation. The data were consistent with the hypothesized fluid-like scattering properties of squid. The contributions from the front and back interfaces of the squid were found to dominate the scattering at normal incidence, while the arms had a significant effect at other angles. The three-dimensional numerical model predictions out-performed the prolate spheroid model over a wide range of orientations. The predictions were found to be sensitive to the shape parameters, including the arms and the fins. Accurate predictions require setting these shape parameters to best describe the most probable squid shape for different applications. The understanding developed here serves as a basis for the accurate interpretation of *in situ* acoustic scattering measurements of squid.
 [http://dx.doi.org/10.1121/1.3701876]

PACS number(s): 43.30.Sf, 43.20.Fn, 43.30.Zk [MCH] Pages: 4461–4475

I. INTRODUCTION

Squids are ecologically and commercially important marine organisms. They support many near-shore and pelagic fisheries and transfer energy across different trophic levels through their roles as both predator and prey (Rodhouse, 2001; Santos *et al*., 2001; Payne *et al*., 2006). However, conventional net-based survey methods are inherently sparse in both space and time, and suffer from the problem of avoidance and damage to the animals. These problems are exacerbated for squid due to their highly variable abundance, rapid speed, and effective avoidance capabilities (Starr *et al*., 1998; Boyle and Rodhouse, 2005). Acoustic scattering techniques, on the other hand, can provide synoptic data over relevant temporal and spatial scales with high resolution (Medwin and Clay, 1998), and do not suffer from the problem of avoidance or net-induced damage to the animals, though accurate interpretation of acoustic data remains a key challenge. The combination of conventional net-tow and acoustic scattering data has the potential to provide more accurate squid stock assessment and distribution.

The scattering of sound from any given target is highly complex, varying strongly with the size, shape, angle of orientation relative to the incident acoustic wave, material properties of the target, and the acoustic frequency (Medwin and Clay, 1998). Successful interpretation of acoustic scattering data usually requires a combination of physics-based target strength (TS) modeling, either analytical or numerical, and comprehensive laboratory measurements for verification of the model predictions (Medwin and Clay, 1998). The frequency response of a particular target provides one avenue for remote discrimination and characterization. However, many acoustic surveys continue to rely on narrowband techniques, which do not systematically provide sufficient information for accurate discrimination, classification, and characterization of the insonified scatterers. Recent advances in broadband acoustic scattering instrumentation and techniques, resulting in greater spectral coverage of the scattered frequency response, provide a new opportunity to develop more effective target discrimination and classification algorithms (Foote *et al*., 1999, 2000; Stanton, 2009; Stanton *et al*., 2010; Lavery *et al*., 2010).

The acoustic backscattering from squid has been the focus of laboratory studies for decades. Early on, it was concluded that the TS of live squid is significantly different from dead specimens, dominated by the fluid-like body, and varies strongly with the orientation of the squid relative to the incident sound wave (Arnaya *et al*., 1989; Arnaya and Sano, 1990; Kajiwara *et al*., 1990; Starr *et al*., 1998). Based on these findings, live squid have been used in most recent experiments, and the TS variation with angle of orientation has been one of the primary goals of a number of studies (Kawabata, 1999, 2001, 2005; Kang *et al*., 2005; Benoit-Bird *et al*., 2008). In addition to the above narrowband measurements, a limited number of broadband measurements of scattering from squid using artificial toothed-whale echolocation signals have also been conducted (Madsen *et al*., 2007; Au and Benoit-Bird, 2008). However, detailed spectral analyses were not available for these studies, and data were collected only at normal and end-on incidence.

Several acoustic scattering models have been proposed for squid based on its fluid-like, weakly scattering properties. These models include the exact modal-series solution for a liquid prolate spheroid (Arnaya and Sano, 1990; Mukai

et al., 2000), the Kirchhoff ray-mode model (Kang *et al*., 2006), and the distorted-wave Born approximation (DWBA) formulation applied analytically using a simple prolate spheroid shape (Mukai *et al*., 2000) or numerically with a realistic three-dimensional geometry (Jones *et al*., 2009). The development and assessment of these models are particularly important for the study of squid, since controlled acoustic experiments are not practical for many commercially important species of squid due to the difficulties in specimen handling. Although all of the above models have been compared with narrowband experimental data, the models have not been tested over a broad range of frequencies and angles of orientation due to the lack of experimental data.

To allow the study of both the frequency and angular dependence of the acoustic scattering from squid, a controlled laboratory backscattering experiment has been conducted on live squid (*Loligo pealeii*) using broadband signals (60–103 kHz) with data collected over the full 360° of orientation in the lateral plane, in <1° increments. Data collected in this study have been compared to model predictions given by the analytical DWBA prolate spheroid model and the three-dimensional DWBA numerical model which takes into account inhomogeneous, fluid-like material properties, and realistic squid shape, obtained using computed tomography (CT) scans (Jones *et al*., 2009).

It is generally understood that the scattering of squid is dominated by its fluid-like body construction (the muscles) with material properties very close to sea water (Iida *et al*., 2006; Kang *et al*., 2006). However, there remain questions over the scattering contribution from other body parts, including the chitinous beak and pen (gladius), eyes, internal organs such as the liver and gonads, skulls, and even the thickened suckers on the arms (Goss *et al*., 2001; Madsen *et al*., 2007; Benoi-Bird *et al*., 2008). Taking advantage of the broadband signals used in this study, pulse compression processing (Chu and Stanton, 1998) has been used to identify the dominant scattering mechanism of squid at different angles of orientation. This time-domain technique has been applied successfully in previous studies of scattering from zooplankton, fish, squid, and shells (Stanton *et al*., 1998b, 2000; Stanton and Chu, 2004; Reeder *et al*., 2004; Au and Benoit-Bird, 2008).

This study (1) provides a set of broadband acoustic scattering data from live squid with full coverage of angle of orientation in the lateral plane, (2) assesses the performance of two DWBA-based models, (3) identifies the observed dominant scattering mechanisms of live squid for important orientations, and (4) investigates the importance of squid arm posture and fin shape in determining the scattering. This study also gives insight into the application of the models under possible field conditions.

II. EXPERIMENTAL METHODS

A. Squid used in the experiment

Longfin inshore squid, *Loligo pealeii,* collected by the Marine Resource Center at the Marine Biological Laboratory, Woods Hole, MA, were used in the experiment. This coastal epipelagic species has a long, slender body and large fins in proportion to its mantle length (Roper *et al*., 1984). The animals were freshly-caught (<1 day) by trawl nets and kept in a tank filled with flowing chilled seawater. Healthy individuals were selected by visual inspection with the requirement that the body length has to satisfy the far-field criteria in the geometry of the experimental setup. A total of seven individuals (Table I) were used and nine successful acoustic measurements were made.

Spiral computed tomography (SCT) images obtained by Jones *et al*. (2009) were used in this study to produce realistic digital representations of the three-dimensional shape of the squid. The SCT images were obtained for a single, live, anesthetized squid and a single, dead, previously frozen squid, both of the same species as those used in the experiment. These scanned images were subsequently reconstructed and interpolated onto a $0.5 \times 0.5 \times 0.5$ mm grid for modeling operations. To investigate the scattering contributions of different body parts and construct appropriate squid shapes to facilitate data-model comparison, the shape of the fins and arms of the squid in the SCT images were further modified (Secs. III B and III C). The volume representations used for the modeling were also scaled anisometrically and interpolated onto the same $0.5 \times 0.5 \times 0.5$ mm grid to match the morphometric dimensions of each of the individuals measured in the experiment.

TABLE I. Dimensions and ranges of angle of orientation for the squid used in the acoustic backscattering measurements. All dimensional measurements were conducted when the animal was dead after the acoustic experiment was completed. The total length is the length from the tip of the mantle to the tip of the arms when the squid is placed flat on a surface. The mantle width is the width of the widest portion of the mantle on the dorsal side. The mantle length is the length between the two ends of the mantle on the dorsal side. Two numbers in the measured angle of orientation indicate that acoustic measurements were conducted twice on the same individual. The calculated weight was calculated using the published length-weight relationship for *L. pealeii* (Lange and Johnson, 1981).

Animal #	Mantle length (cm)	Mantle width (cm)	Total length (cm)	Range of angle of orientation measured (°)	Calculated weight (g)
0807 a	12.2	3.3	16.2	803/742	55.8
0812 a	7.7	2.1	12.5	722	20.7
0814 a	6.8	2.3	15.0	759.5/768.5	15.9
0819 c	10.8	2.8	17.0	733	43.0
0822 a	11.4	3.0	18.0	751.5	48.3
0825 a	11.4	3.0	17.5	412.5	48.3
0826 b	9.6	2.8	16.6	285	33.3

B. Tank and instrument setup

The acoustic scattering experiment was conducted in an indoor flume tank at the Woods Hole Oceanographic Institution. The tank was 23 m long and 1.2 m wide on a side. The tank was filled to a depth of 1 m with seawater at 21 °C [Fig. 1(a)]. The seawater was filtered by a 5 -μm filter. The experimental setup, the tank, and the transducers were identical to those used in Stanton and Chu (2004). Most of the other instruments were the same as those used in Lavery and Ross (2007). The pulse-echo system consists of a power amplifier (custom made at the Woods Hole Oceanographic Institution), a pair of identical transducers (Reson, Goleta, CA, TC2116), an integrated preamplifier and bandpass filter (RITEC Inc., Warwick, RI, Model BR-640 A), and a National Instruments (NI, Austin, TX) data acquisition system (NI Model PXI-1000B) with an embedded computer controller (NI Model PXI-8175 running Windows 2000).

The pulse-echo system was controlled by custom-written LabVIEW software modified from the one used in Lavery and Ross (2007) to display the envelope of the compressed pulse output (CPO) with background reverberation subtracted (see Sec. II E) in real-time and to control the angle of orientation of the squid through the stepper motor and the associated controller (Pontech, Rancho Cucamonga, CA, STP101). An amplitude-shaded linear chirp signal (see Sec. II D) was loaded, sent through the power amplifier, and transmitted by the transmit transducer. The raw received signal was pre-amplified before being recorded. The transmit signal, as measured both at the input of the power amplifier and through a –40-dB signal sampler (RITEC Inc., Model SS-40) at the output of the power amplifier, and the raw received signals (including the echoes from the squid and reverberation from the tank) were all sampled at 2 MHz throughout the experiment. The center-to-center separation between the transmit and receive transducers was 0.34 m and the target-to-transducer distance was 2.71 m, resulting in a 7.2° deviation from true backscattering. This deviation was not accounted for in the modeling.

C. Experimental procedure

Each squid was anesthetized by soaking the animal in a 0.1% MgCl solution for a 10–15 min period, depending on the condition of each individual (Mooney *et al.*, 2010). The anesthetized animal was then pierced and suspended by a Y-shaped harness made with three 4-lb monofilament lines [Fig. 1(b)]. The definition of squid orientation shown in Fig. 1(b) is followed throughout this paper. The harness was subsequently fixed onto a tetrahedron-shaped rotation frame consisting of three 10-lb monofilament lines, a T-shaped frame above water, and a pivot on the bottom of the tank [Fig. 1(a)].

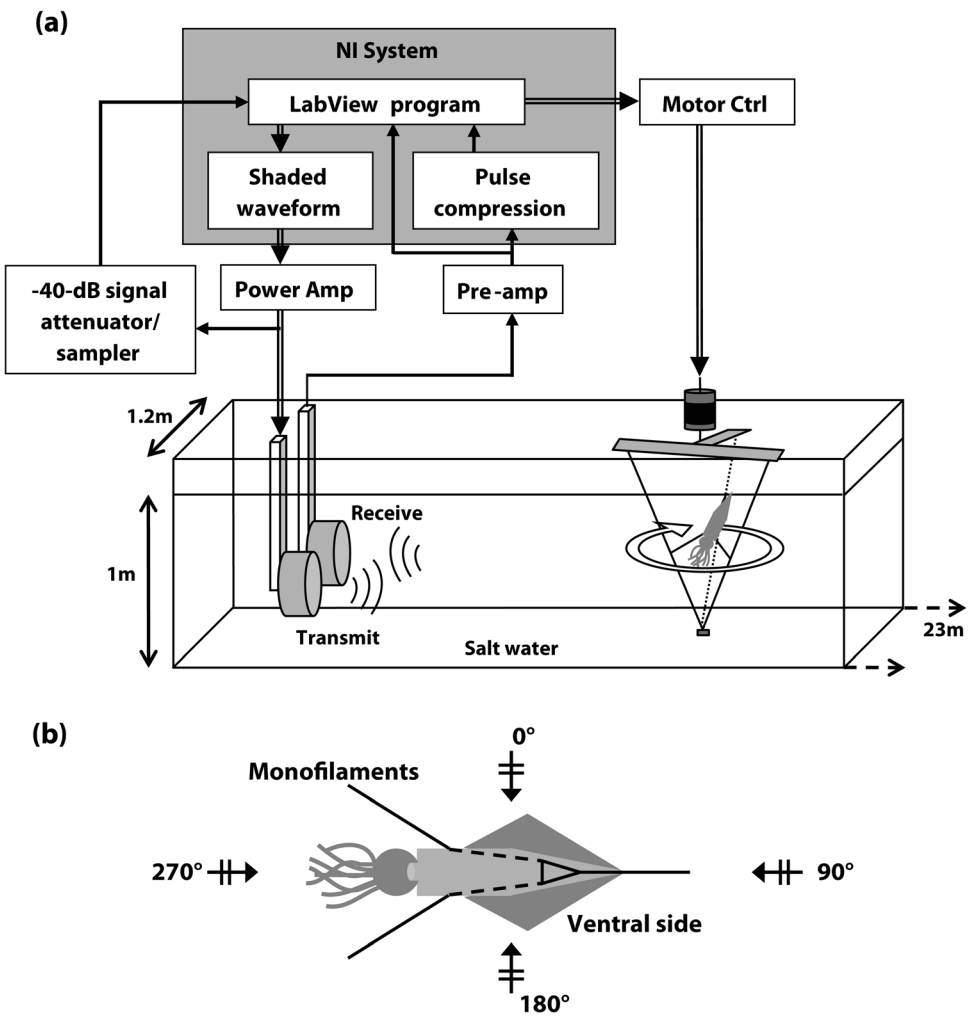

FIG. 1. (a) The pulse-echo system and experimental setup. The shaded box represents the NI system containing the central LabVIEW control program. (b) Tethering system used in the experiment and the definition of angle of orientation relative to incident acoustic signal. Solid lines represent monofilament lines outside of the squid body. Dashed lines represent monofilament lines running through the mantle cavity.

This tethering system allowed free movement of the squid mantle and arms without losing control over the designated angle of orientation. All of the monofilament lines were thoroughly wetted and rubbed with soapy water before each measurement. Care was taken in the animal handling and tethering process to maintain the animal underwater at all times to ensure no air bubbles formed on the body surface or in the mantle cavity.

The rotation frame was attached to the stepper motor controlled by the central LabVIEW program and rotated with $<1^\circ$ increments. For each experimental animal, 15–17 acoustic pings were collected at each angle of orientation through two full rotations (720°). The experimental animals were out of anesthetization and alive during the acoustic measurements. In some cases the animal died before a full rotation was completed (Table I) and the experiment was aborted.

D. Acoustic signal analysis and calibration

A chirp signal with a frequency span of 45–105 kHz was used as the transmit signal. The amplitude of the transmit signal was shaded so that the overall system response was more uniform in the spectral domain (Fig. 2). Combined with the frequency-dependent noise levels, this transmit signal resulted in a usable band of 60–103 kHz. The system was calibrated using the procedure described in Stanton *et al.* (1998b). This method involves separating the transducers, aiming them toward each other, and measuring the signals as a result of the acoustic pulse traveling along the direct path between the two. The calibration was performed both before and after the squid measurements.

Taking advantage of the broad signal bandwidth, pulse compression techniques were used to identify the dominant scattering mechanisms of live squid (Chu and Stanton, 1998). The deviation in the CPO envelope from the idealized matched-filter output contains information regarding the scattering properties of the target. Pulse compression

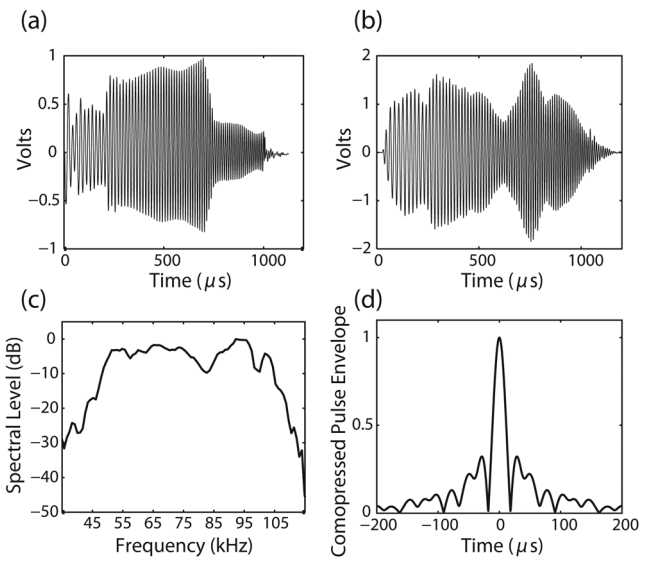

FIG. 2. (a) Transmit signal measured at the output of the power amplifier. (b) Received calibration signal. (c) Spectrum of the received calibration signal. (d) Envelope of the autocorrelation function of the received calibration signal, normalized to the maximum value at 0 μs.

processing of broadband signals has the advantage of increasing the time-domain resolution and signal-to-noise ratio (SNR). This is of particular importance for identifying the dominant scattering mechanisms for weak scatterers, such as squid.

In this experiment, the received echo signal was compressed in time by cross-correlating the echo with the received calibration signal. The mainlobe width of the envelope of the autocorrelation function [Fig. 2(d)] limits the finest spatial resolution achievable by the system. The normalized height of the first sidelobe is 0.321. Sidelobes can introduce spurious artificial echoes in the analysis and must be considered carefully when interpreting scattering features.

E. Subtraction of background reverberation

Because the experiment was conducted in a long, narrow tank, background reverberation had to be subtracted off to identify and isolate the echoes from the squid. Two sets of 200 pings of background reverberation (with no squid in the tethering system) were collected immediately prior to the acoustic measurements. Another 200 pings of background reverberation were collected immediately after the acoustic measurement, when the situation permitted.

The pre-experiment background reverberation signals were coherently averaged and stored as the background reverberation reference. During the backscattering experiment, unmodified raw signals consisting of both the squid echoes and background reverberation were collected. The echoes from the squid were isolated by subtracting the background reverberation reference from the raw receiving signals. Background reverberation signals other than those used to form the background reverberation reference were used for assessing the background noise level in the data analysis (see Appendix A for details).

III. THEORY AND MODELING

A. Basic definitions

Acoustic scattering from an object in the far-field can be expressed as

$$P_{scat} = P_0 \frac{e^{ikr}}{r} f, \tag{1}$$

where P_0 is the pressure amplitude of the incident wave, r is the distance from the object to the receiver, and f is the scattering amplitude. The scattering amplitude fully describes the acoustic scattering characteristics of a target and is a measure of the efficiency with which a target scatters sound. It is a function of the acoustic wavenumber k ($=2\pi/\lambda$, where λ is the acoustic wavelength), and the target's shape, size, angle of orientation, and material properties, such as the mass density ρ, and sound speed c.

As the dynamic range of the scattered signals is typically very large, a logarithmic measure of the backscattering amplitude is used, defined as target strength (TS), expressed in units of decibels (dB) relative to $1\,\mathrm{m}^2$, and given by $\mathrm{TS} = 10\log_{10}|f_{bs}|^2 = 10\log_{10}\sigma_{bs}$, where $\sigma_{bs} \equiv |f_{bs}|^2$ is the

differential backscattering cross section, and f_{bs}, or backscattering amplitude, is the scattering amplitude evaluated in the backscattering direction.

B. Distorted-wave Born approximation formulation: Application to squid

The scattering amplitude for any weakly scattering object can be modeled in the far-field using the DWBA in which the total pressure field within the scatterer is approximated by the unperturbed incident wave field, with the wavenumber replaced by the wavenumber inside the scatterer (Morse and Ingard, 1987; Chu *et al.*, 1993; Stanton *et al.*, 1993). With this approximation the backscattering amplitude can be written as

$$f_{bs} = \frac{k_1^2}{4\pi}\int (\gamma_\kappa - \gamma_\rho) e^{2i\mathbf{k}_v\cdot\mathbf{r}_v} dv. \tag{2}$$

In the above formulation, the subscript "1" indicates parameters of the surrounding medium, while the subscript "v" indicates parameters of the scattering body. The term $\mathbf{k}_v$ is the wavenumber vector within the scattering volume, and $\mathbf{r}_v$ is the position vector of any volume element. The terms γ_κ and γ_ρ are defined in terms of the compressibility κ and density ρ, and can be written in terms of the density contrast g_v ($= \rho_v/\rho_1$) and sound speed contrast h_v ($= c_v/c_1$) between the medium and the scattering object, i.e.,

$$\gamma_\kappa \equiv \frac{\kappa_v - \kappa_1}{\kappa_1} = \frac{1 - g_v h_v^2}{g_v h_v^2}, \tag{3}$$

and

$$\gamma_\rho \equiv \frac{\rho_v - \rho_1}{\rho_v} = \frac{g_v - 1}{g_v}. \tag{4}$$

This integral can be solved analytically for simple objects, such as spheres and cylinders (Stanton *et al.*, 1998a), and is particularly useful for numerically modeling the scattering from bodies with arbitrary shapes (Lavery *et al.*, 2002) and material properties (Jones *et al.*, 2009). In this study, two DWBA-based models are compared: (1) an analytical model with a simple geometry (smooth prolate spheroid) and homogeneous material properties, and (2) a numerical model which involves three-dimensional digitization of the squid and inhomogeneous material properties.

1. Analytical DWBA prolate spheroid model

The prolate spheroid geometry is a first order approximation to the elongated shape of the squid (Arnaya and Sano, 1990; Mukai *et al.*, 2000). The analytical DWBA solution for a prolate spheroid geometry [derived by D. Chu and given in Johnson (1993)] is reproduced here for reference

$$f_{bs} = \frac{k_1^2 a^2 L(\gamma_\kappa - \gamma_\rho)}{2} \frac{j_1\left(k_v\sqrt{4a^2\sin^2\theta + L^2\cos^2\theta}\right)}{k_v\sqrt{4a^2\sin^2\theta + L^2\cos^2\theta}}, \tag{5}$$

where a is the semi-minor axis (equatorial radius), L is the major axis (twice the polar radius), θ is the polar angle from the major axis, and j_1 is a spherical Bessel function of the first kind of order one.

In this study, the width ($2a$) of the prolate spheroid was set to match the measured maximum width of each squid used in the experiment. The length of the prolate spheroid, L, was determined by matching the total volume of the homogeneous (no sea-water-filled cavities in the mantle cavity) squid digital representation to the volume of the prolate spheroid. Details of the inhomogeneities in the squid body and the scaling issues can be found in Jones *et al.* (2009).

2. Three-dimensional DWBA numerical model

The three-dimensional DWBA numerical model calculates the scattering response of an arbitrarily-shaped object by numerically integrating the phase change contributed by local material property variation over a digital volume representation of this object (Lavery *et al.*, 2002; Jones *et al.*, 2009). This is of particular interest in modeling the acoustic scattering from squid, since the outer shape is complex, particularly in the arms, and the body contains sea-water-filled cavities.

The SCT images obtained by Jones *et al.* (2009) were used as the baseline digital representations of squid in this study. The arms-splayed squid volume was taken directly from the actual scan of the anesthetized specimen, while the arms-folded squid volume was constructed by hybridizing the arms of the dead specimen with the mantle of the anesthetized specimen. The orientation of the squid in the digital representation was such that the center line of the mantle was parallel to the z-axis of the digital volume, with the x-y plane representing cross-sectional slices along the squid's longitudinal axis.

In addition to the above manipulations, the shape of the arms and the fins were further modified for modeling purposes in this study. Unless otherwise specified, the mantle volume used in the following three-dimensional DWBA numerical modeling was the mantle of the anesthetized specimen with the fins digitally removed (see Sec. III C), because the modeling results using this mantle shape have the best agreement with the experimental data (see Sec. IV B). To facilitate data-model comparison, the mantle width and total length of the digital squid volume were scaled to match the maximum mantle width and total length, respectively, of the experimental animal.

3. Modeling parameters

In modeling the scattering of weak scatterers such as squid, it is known that small variations of g (density contrast) and h (sound speed contrast) can give rise to TS variation as large as 20 dB (Chu *et al.*, 2000). However, there are no measurements available for the material properties of *L. pealeii*. Therefore, the tissue material properties of the Japanese flying squid (*Todarodes pacificus*) ($g = 1.043$, $h = 1.053$, Iida *et al.*, 2006; Jones, 2006) were used instead for both the analytical DWBA prolate spheroid model and the three-dimensional DWBA numerical model in this study.

Another important modeling consideration is the digitization resolution of the modeled scatterer volume (characterized by the maximum dimension of the digitization voxel, l_V) compared to the acoustic wavelength. A value of 20 for the ratio λ/l_V is generally required for properly estimating the acoustic scattering of fluid-like elongated zooplankton (Stanton and Chu, 2000). Based on this principle, the numerical model output was constrained below 150 kHz, corresponding to a λ/l_V ratio of 20 with the digital volume resolution of $l_V = 0.5$ mm. The highest frequency of the chirp signal used in the experiment was 105 kHz, which resulted in $\lambda/l_V = 28.57$.

C. Model predictions

The comparison of the model predictions given by the analytical DWBA prolate spheroid model and the three-dimensional DWBA numerical model using realistic squid shapes illustrates the baseline difference between models with simple versus complicated geometries. In addition, the three-dimensional DWBA numerical model has made it possible to investigate the contribution from individual body parts by digitally modifying the shape of the squid volume. Of particular importance are the shapes of the fins and the arms, which were modified or randomized to obtain the best agreement with the data (Figs. 3–8).

1. Comparison of model predictions for the analytical DWBA prolate spheroid model and the three-dimensional DWBA numerical model

The TS predictions given by the analytical DWBA prolate spheroid model and the three-dimensional DWBA numerical model are compared for both the angular dependence (Fig. 3) and the frequency response (Fig. 4). At normal incidence, the TS predictions for both models reach the maximum with comparable values. When the incident angle deviates from normal incidence, the analytical DWBA prolate spheroid model predictions drop much more rapidly than the three-dimensional DWBA numerical model predictions.

The analytical DWBA prolate spheroid model predictions also contain structured nulls in both the TS versus frequency and TS versus angle responses (Figs. 3 and 4), produced by constructive and destructive interference accentuated by the smoothness and symmetrical shape of the prolate spheroid. In addition, the analytical DWBA prolate spheroid TS predictions are slightly higher than those of the three-dimensional DWBA numerical model in the Rayleigh scattering region at all angles of orientation (Fig. 4). This is due to the fact that the prolate spheroid was scaled by matching the spheroid volume to the volume of homogeneous digital squid representation with the fins. This volume is larger than the volume of the inhomogeneous, no-fin squid shape used in the three-dimensional DWBA numerical model.

2. Contribution of individual body parts

The flexibility of the three-dimensional DWBA numerical model in incorporating complicated geometries facilitates the investigation of the scattering contributions from individual squid body parts, such as the fins and the arms. To understand the impact of the fins on the backscattering, numerical model predictions were made using the same folded arms but with the original asymmetric fins and with the fins digitally removed (Fig. 3). The scattering contribution of the fins is most prominent at the "shoulders" of the curve around 20°–40° from normal incidence for higher frequencies (indicated by the arrow in Fig. 3), and is less important at angles far from normal incidence. The asymmetric scattering pattern on either side of normal incidence is the result of the asymmetric shape of the original fins on either side of the squid.

The posture of the arms also has a significant effect on the scattering prediction across all angles of orientation (Fig. 5). In Fig. 5, the model CPO envelope was produced by cross-correlating the model impulse response with the

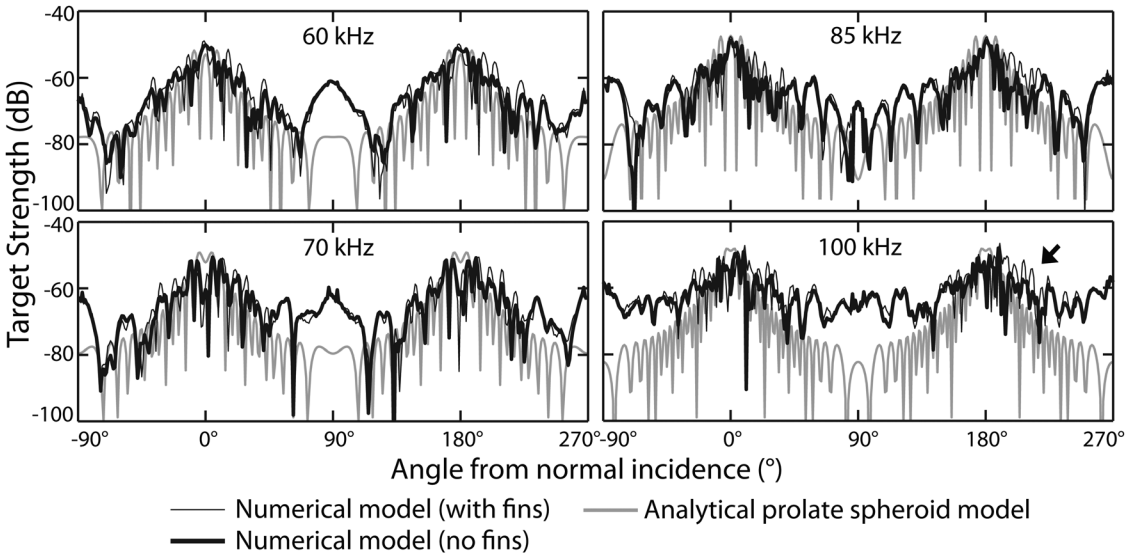

FIG. 3. TS prediction versus angle of orientation at four frequencies (60, 70, 85, and 100 kHz) for the three-dimensional DWBA numerical model using arms-folded squid shapes with and without the fins, and the analytical DWBA prolate spheroid model. The arrow indicates the scattering contribution from the fins.

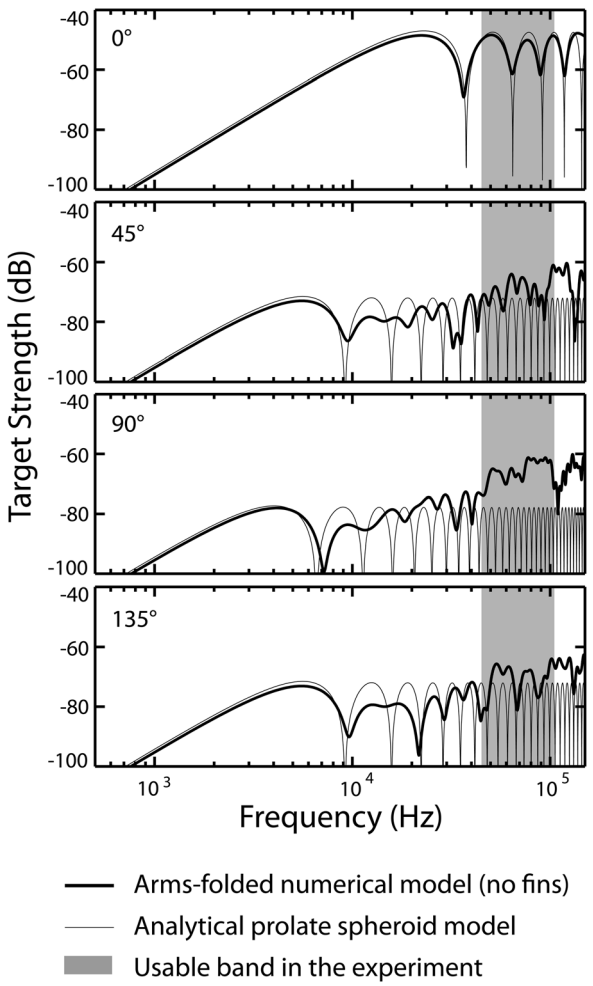

FIG. 4. TS predictions versus frequency for the three-dimensional DWBA numerical model using arms-folded squid shape and the analytical DWBA prolate spheroid model at four angles of orientation (0°, 45°, 90°, 135° from normal incidence). The usable band (gray area) in the experiment lies entirely in the geometric scattering region.

autocorrelation function of the transmit signal (Chu and Stanton, 1998). The model impulse response was obtained by applying an inverse Fourier transform on the model spectra from 100 Hz to 150 kHz, in 100 Hz increments. A strong sinusoidal pattern corresponding to the squid arms is observed in the modeled CPO envelopes in both plots. The scattering from the arms is stronger in the arms-splayed case. Since the two shapes only differ in the arm posture and have the same mantle shape, this result shows the importance of the arm posture on the acoustic scattering. A very faint secondary sinusoidal pattern was also observed resulting from scattering originating at the tail region of the squid.

3. Randomized squid shape

Based on the above observation that the numerical model predictions are highly sensitive to the exact shape of the arms and the fins, these were digitally modified to produce a set of squid shape representations which are reasonably close to the squid shape during the experiment. Fifteen realizations of arms were generated to resemble the "loosely-folded" arm posture of the squid resting in the harness (see the images included in Fig. 8). Three fin shapes were used in combination with these randomly generated arms to produce a set of hybrid randomized squid shapes to facilitate the data-model comparison.

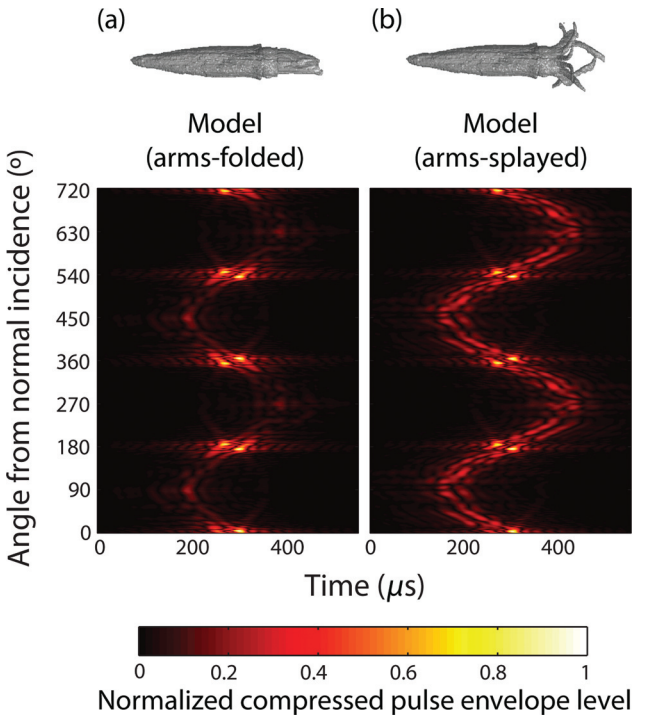

FIG. 5. Compressed pulse output envelope of the three-dimensional DWBA numerical model using two fixed squid shapes through two full rotations (720°): (a) arms-folded configuration and (b) arms-splayed configuration. The CPO envelopes are normalized to the maximum envelope value in each of the plots. The strong sinusoidal pattern in both plots corresponds to the location of the squid arms during the rotation.

The shape of each randomized arm was determined by three points: the initial, middle, and end points in the three-dimensional space. The space was defined such that the z-axis is parallel to the longitudinal axis of the squid body, with $z = 0$ being the surface joining the arms and the mantle. The (x, y) positions were used to describe the transverse position on a given height of z. Eight initial (x, y) arm positions were manually chosen on the $z = 0$ plane to keep the initial arm positions biologically realistic. The positions of the middle and end points were randomly generated within a pre-defined area on the x-y plane. These areas were defined according to the initial position of each arm to keep the arm shape natural. A spline function was then fitted for the three points of each arm. The arm length was also generated randomly within a biologically reasonable range. Consecutive (x, y, z) points on each arm were then generated according to the spline along the height of the arm. These arm curves were then filled by individual "disks" with decreasing radius toward the tips of the arms. The rim of the disks was randomly roughened to create roughness on the arm surface. The total volume of the arms generated by this procedure was approximately 11%–14% of the total squid volume, which is comparable to the arm/body volume ratio for the two original sets of SCT squid images described in Sec. II A.

Three fin shapes were used: (A) the original asymmetric fins, (B) artificially generated symmetric fins, and (C) no

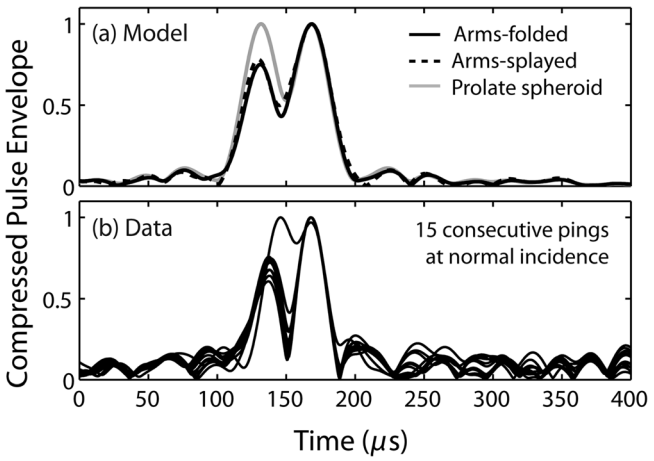

FIG. 6. Temporal characteristics of the scattering at normal incidence. (a) Model predictions given by the three-dimensional DWBA numerical model with arms-folded and arms-splayed squid shapes and the analytical DWBA prolate spheroid model. (b) Experimental data from 15 individual pings overlaid at normal incidence. All CPO envelopes (model prediction and data) were normalized to the maximum value in each model prediction or each ping.

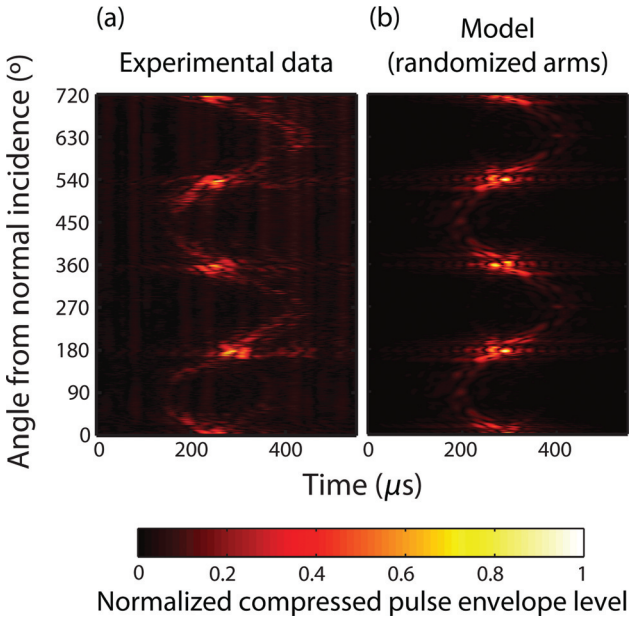

FIG. 7. Compressed pulse output envelope of (a) the experimental data and (b) the three-dimensional DWBA numerical model using a hybrid squid shape with randomized arms over two full rotations (720°). The CPO envelopes are normalized to the maximum envelope value in each of the plots. Faint vertical lines in the experimental data are due to noise not effectively eliminated by the background reverberation subtraction.

fins. Fin volume (A) was directly obtained from the mantle portion of the SCT images of the anesthetized squid. Fin volume (C) was obtained by digitally removing the fins from volume (A). Fin volume (B) was a hybrid volume consisting of a pair of artificially edited symmetric fins and volume (C). The symmetric fins were created by producing a pair of mirror images of a scaled version of a fin retrieved from the SCT images of the dead, frozen squid. These three shapes will be referred to as "original-fins," "symmetric-fins," and "no-fins" mantles throughout the remainder of this paper.

In addition to the variations of the arms and the fins, to make valid comparisons with the experimental data, frequency-dependent noise was added to the scattering amplitude predictions for all of the randomized models. The amount of noise added for a given frequency was calculated based on the background noise level measured during the acoustic measurement. Details of the noise addition procedure are given in Appendix A.

IV. DATA-MODEL COMPARISON

This section discusses the results of data-model comparison for the angular variation of the CPO, TS, and TS averaged over a wide range of angles of orientation. As noted earlier, unless otherwise specified, the fins were digitally removed from all the squid shapes used in the three-dimensional DWBA numerical model. Results are shown for only one representative individual (0822a) throughout this paper.

A. Time domain CPO characteristics

1. CPO at normal incidence

The temporal scattering pattern for both the experimental data and model predictions at normal incidence are compared in Fig. 6. Two distinct peaks were observed in the CPO envelopes of the experimental data and all model predictions. The separations between the two peaks in the model predictions appear to be greater than those in the experimental data. For the experimental data, the separation translates into a spatial distance ranging between 1.74 and 2.45 cm. For the model predictions, the corresponding distance ranges from 2.92 cm for the analytical DWBA prolate spheroid model, to 2.96 and 3.04 cm for the three-dimensional DWBA numerical model using the arms-folded and arms-splayed squid shapes, respectively. The assumed fluid-like scattering property of squid is consistent with the presence of these two dominant peaks in both the experimental data and model outputs. The separation differences between the experimental data and model predictions may be explained by the errors in modeling the actual width of the squid using dimensional measurements performed on dead specimens. The separation differences among the model predictions, on the other hand, are likely induced by the interaction of sidelobes and internal inhomogeneities in the squid body (see Sec. V D).

2. Angular dependence of the CPO

There is reasonably good qualitative agreement in the general scattering pattern across all angles of orientation for the experimental data and model predictions given by the three-dimensional DWBA numerical model using an arbitrarily-chosen realization of the hybrid randomized squid shapes (Fig. 7). In Fig. 7, the last of the 15 pings collected at each angle of orientation was arbitrarily chosen from the experimental data, although the results based on the other pings do not change the general pattern. The hybrid randomized squid shape was used here to model the shape of the squid during the experiment.

The sinusoidal pattern predicted in Fig. 5, corresponding to the location of the squid arms in the rotation, is also observed in the CPO envelopes in Fig. 7 for both the experimental data and the three-dimensional DWBA numerical model predictions. The model predictions also successfully capture the relative scattering strength at off-normal incidence with respect to the maximum level at normal incidence. This result, combined with the scattering characteristics at normal incidence, suggests that the DWBA-based model, which only takes into account the muscular part of the squid body, is capable of explaining a major portion of the scattered energy at off-normal incidence.

B. Angular variation of TS at fixed frequencies

The experimental data are compared to predictions given by the three-dimensional DWBA model using hybrid randomized squid shapes across all angles of orientation at four discrete frequencies: 60, 70, 85, and 100 kHz (Fig. 8). These four frequencies are chosen because they are evenly spaced across the usable band and are not in the high-noise band around 75 kHz in the middle of the spectrum. Frequency-dependent noise was added to the model predictions as mentioned in Sec. III C. Experimental data or model predictions with TS values lower than the background noise reference level are omitted in Fig. 8, resulting in the cut-off pattern near the bottom of each plot.

In general, the model predictions agree well with the experimental data across all angles of orientation with the best correspondence at 70 and 85 kHz. Among the three types of mantle shapes used, the no-fins mantle (right column) shows the best agreement with the experimental data. This may be associated with the resting posture of the squid during the experiment, in which the fins hung downward and wrapped against the mantle and resulted in a shape that is similar to the no-fins mantle. The shape of the fins has a pronounced effect on the scattering pattern at the shoulders near normal incidence (around 20°–40° from normal incidence, as indicated by the arrow in Fig. 8). This effect is the most prominent on one side of normal incidence in the model predictions using the asymmetric-fin mantle (left column), and less prominent and more symmetric for the model predictions using the symmetric-fin mantle (middle column).

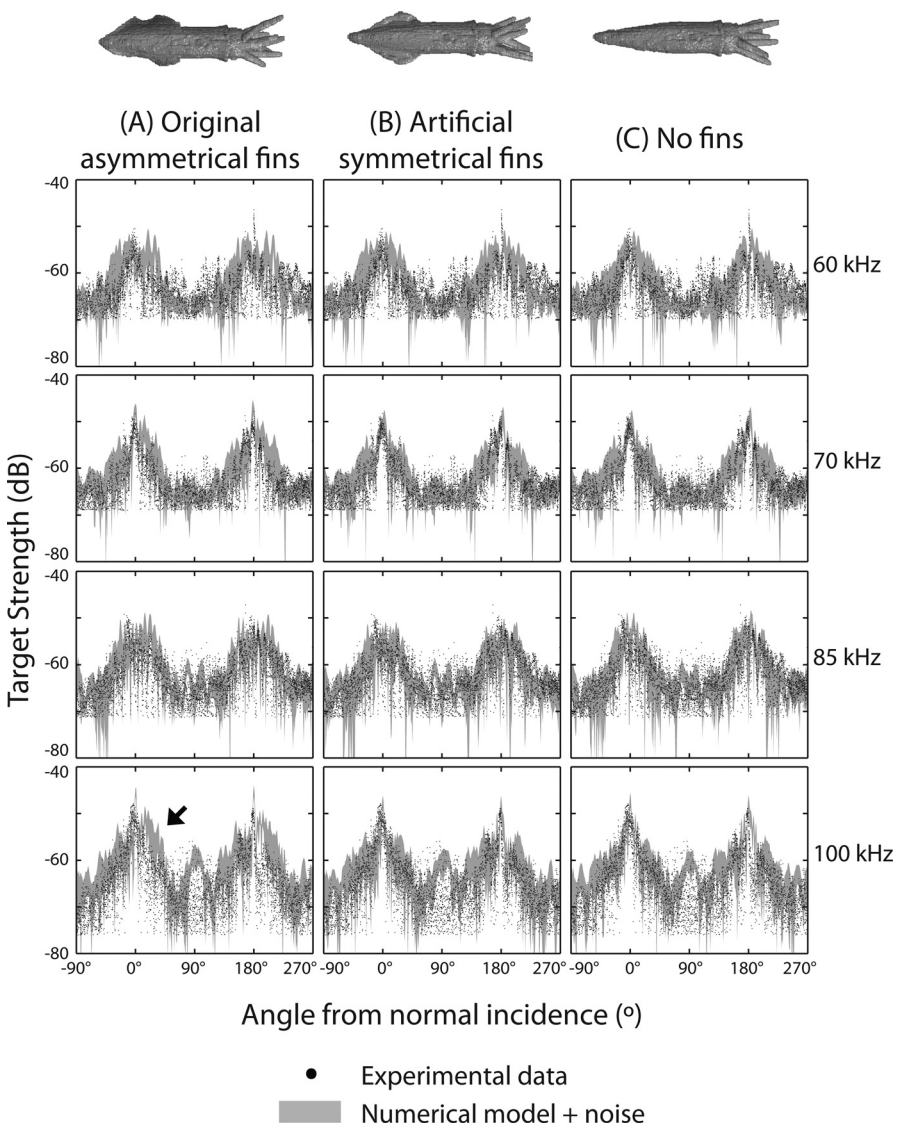

FIG. 8. Data-model comparison of TS versus angle of orientation at four frequencies (60, 70, 85, and 100 kHz). Hybrid randomized squid shapes with three fin shapes were used in the three-dimensional DWBA numerical model: (A) original asymmetric fins, (B) artificial symmetric fins, (C) no fins. The experimental data are represented by dots. The gray area indicates the range of ±1 standard deviation from the mean of the model predictions. The arrow indicates the scattering contribution of the fins. The cut-off pattern near the bottom of each plot is resulted from omitting experimental data and model predictions lower than the noise threshold.

No prominent shoulders are observed in the experimental data at any frequencies.

Similar data-model comparisons were also carried out to assess the performance of the prolate spheroid model (Appendix B). As expected, even with the same amount of noise added, the prolate spheroid model still underestimates the TS at angles far away from normal incidence. This result is consistent with the results in Jones *et al.* (2009).

C. Model predictions of TS averaged over angle-of-orientation distribution

To assess the model performance under possible field conditions, averaged TS predictions in both the dorsal-ventral and lateral planes given by the analytical DWBA prolate spheroid model and the three-dimensional DWBA numerical models are compared in Fig. 9. Experimental data, which are only available in the lateral plane, were also averaged and compared to the model predictions [Fig. 9(b)]. At each angle, experimental data from all pings were used in the average. The averages were obtained assuming the angles of orientation are normally-distributed with a mean angle μ and a standard deviation σ. The calculations were limited to within ± 2 standard deviations from the mean. Averages were performed on the differential backscattering cross sections σ_{bs} and converted to TS. Figure 9 shows TS, in contrast to the reduced TS (RTS) shown in Fig. 10 in Jones *et al.* (2009). Since the choice of the normalizing length factor (mantle length or total length of the squid) affects the RTS values, all comparisons here were done based on TS.

The dorsal-ventral plane TS averages are relevant to data collected by downward-looking sonars for fisheries applications. A previously reported angle-of-orientation distribution for free-swimming squid ($[\mu, \sigma] = [-4°, 11.1°]$) was used (Arnaya *et al.*, 1989). TS predictions were also averaged over three other angle-of-orientation distributions with off-normal mean angles ($\mu = -20°, -40°, -60°$) and identical standard deviation ($\sigma = 10°$). The angle of orientation was defined as a negative value when the arms were placed under the horizontal axis [see examples in Kang *et al.* (2005)].

In this plane, the averaged TS predictions given by the three-dimensional DWBA numerical model are generally higher than the predictions given by the analytical DWBA prolate spheroid model for most of the frequencies. The differences between these two models are larger when the angle-of-orientation distributions are dominated by off-normal angles. Although no experimental data were available to assess the model performances, the analytical DWBA prolate spheroid model is likely to under-predict the actual TS averages, as suggested by the results of the data-model comparison in the lateral plane (see below) and the conclusions in Jones *et al.* (2009). The three-dimensional DWBA numerical model predictions using different squid shapes remain close to one another across the frequencies, except for in the >75 kHz region when the symmetric-fins mantle is used. This elevation in the TS is likely due to the constructive interference produced by the horizontally-extended symmetrical fins that are perpendicular to the incident wave in this geometry.

The TS averages in the lateral plane are relevant to data collected by sonars looking near horizontally such as the outer beams of multibeam sonar systems. TS predictions were averaged over several angle-of-orientation distributions with different mean values ($\mu = 0°, \pm 20°, \pm 40°, \pm 60°$) and the same standard deviation ($\sigma = 10°$). The angle of orientation follows the definition in Fig. 1(b).

In this plane, when the angle-of-orientation distribution is dominated by near-normal angles ($\mu = 0°$), all model predictions gave similar spectral structures and averaged TS values, and their performance cannot be distinguished by the experimental data [Fig. 9(b)]. The differences among the model predictions become larger as the mean angle deviates from normal. The three-dimensional DWBA numerical model using hybrid squid shapes with randomized arms generally generates higher TS averages compared to the predictions made using other squid shapes with folded arms. TS averages predicted using the three arms-folded squid shapes are similar, except for the elevated values in the >80 kHz region of the $\mu = 40°$ and $\mu = 20°$ cases when the squid shape with the original asymmetrical fins was used. These elevated values are likely produced by the specific fin orientation with respect to the sonar, as discussed in Secs. III C and IV B.

Although the three-dimensional DWBA numerical model predictions were not able to fully reproduce the experimental data across the usable frequency band for all angle-of-orientation distributions, the predictions given by different squid shapes appear to collectively bound the experimental data, except for a subset of the data near end-on incidence ($\mu = \pm 60°$). The predictions made using the hybrid randomized squid shapes do not necessarily give the best agreement with the data. However, the distribution of the predicted TS values using these hybrid randomized squid shapes better captures the distribution of the experimental data than the predictions made using all other squid shapes (not shown). This observation reflects the importance of knowing the squid shape accurately when predicting the TS, as well as the complexity of the scattering process, especially for off-normal angles of orientation.

In the lateral plane, the analytical DWBA prolate spheroid model predictions drop much more rapidly compared to the predictions of the numerical model when the angle of orientation deviates from normal incidence (Fig. 3). This rapid drop leads to the generally lower averaged TS when the angle-of-orientation distributions are dominated by off-normal angles [Fig. 9(b)]. The analytical DWBA prolate spheroid model underestimated the TS averages in the $\mu = \pm 40°$ and $\mu = \pm 60°$ cases. In the $\mu = \pm 20°$ case, this model appears to correspond well with the experimental data. However, the distribution of the predicted TS values of the prolate spheroid model in these cases were not consistent with the distribution of the experimental data (not shown), and the correspondence was merely a coincidence.

V. DISCUSSION

A. Model performance

Results of the data-model comparison show that the three-dimensional DWBA numerical model, which takes into account only the fluid-like soft tissue in the squid body, is

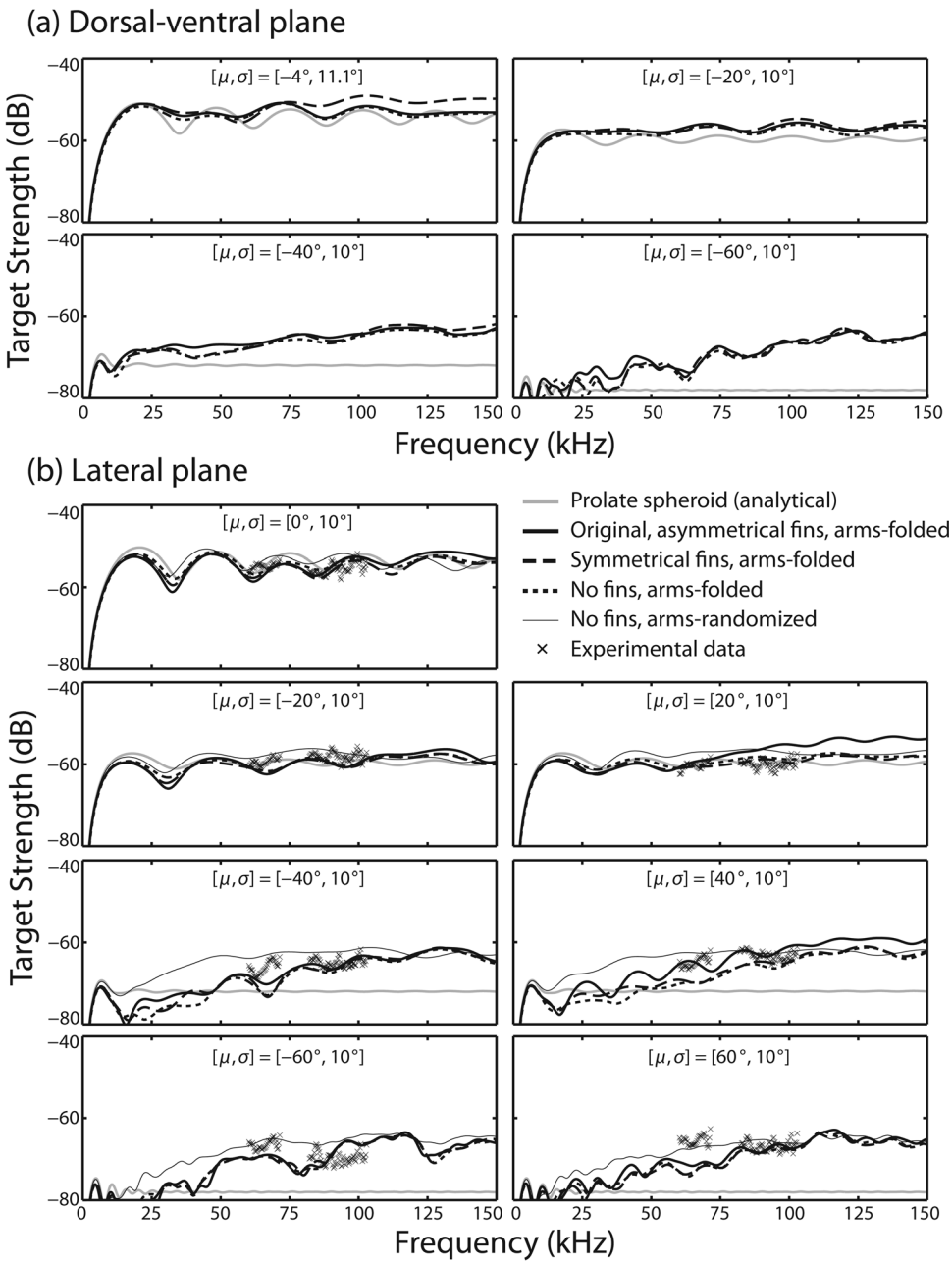

FIG. 9. Averaged TS versus frequency for the experimental data, the analytical DWBA prolate spheroid model, and the three-dimensional DWBA numerical model using both fixed and hybrid randomized squid shapes in two planes (data only available in the lateral plane). All averages were done in the linear domain over ±2 standard deviations (σ) from the mean angle (μ) and converted to TS. (a) Averages in the dorsal-ventral plane. (b) Averages in the lateral plane.

capable of capturing the observed dominant scattering characteristics of squid. In particular, the presence of two dominant peaks at normal incidence in the CPO envelopes in the experimental data is consistent with the model predictions (Fig. 6), and the pattern of the time domain CPO envelopes and model TS predictions across all angles of orientation correspond reasonably well with the experimental data (Figs. 7–9).

Results of the data-model comparison also show that the three-dimensional DWBA numerical model, compared to the analytical DWBA prolate spheroid model, is capable of giving better TS estimation once averaged over an ensemble of predictions made using a set of squid shapes with randomized arms at fixed frequencies (see Sec. IV B and Appendix B). This result is consistent with the previous conclusion reached by Jones *et al*. (2009) and illustrated in Fig. 9 of that paper. The three-dimensional DWBA numerical model also produces better predictions for TS averaged over a range of angles of orientation at different frequencies (Fig. 9). However, this numerical model was not able to predict the measured TS spectral curves on a ping-by-ping basis (not shown). This may be explained by the fact that the spectral structure of the TS is highly sensitive to the precise size, shape, orientation, and material properties, including detailed internal inhomogeneities, of the animals (Stanton *et al*., 1998a), as well as the scattering contribution from other sources in addition to the muscle tissue. The influence of these parameters on acoustic scattering from squid is discussed in more detail below.

B. Squid tissue material properties

In this study, the soft-tissue material properties of *T. pacificus*, a similar species in the Pacific Ocean, have been used to model the scattering from *L. pealeii*. This was done under the assumption that these epipelagic squid species have similar muscle material properties, which are closely

related to the habitat and ecological role of the species (Seibel *et al.*, 2004). Different material properties will be required to predict acoustic scattering from other more distantly-related squid species, such as the larger and highly muscular jumbo squid, *Dosidicus gigas,* or the mid-water, ammoniacal squid with generally lower muscle density (O'Dor, 2002). In addition, variation of local material properties may be required to model the scattering from some species. For example, unlike the thickened flesh suction cups found in *L. pealeii*, each of the suction cups of *D. gigas* has a chitinous ring of teeth, which may have different material properties than the muscle.

C. Scattering contribution from other potential sources

The DWBA-based models employed in this study to predict scattering from squid only consider the fluid-like soft tissue in the squid body and do not account specifically for the scattering contribution from other body parts, such as the skull, chitinous beak, eyes, and other internal organs. The model predictions were able to reproduce the observed dominant scattering features in the time domain and give reasonable estimation of the observed TS (Figs. 6–9). These results show that, at least in the lateral plane, the majority of the scattering energy can be explained by the fluid-like scattering properties of the tissue, and the contributions from other potential body parts are relatively insignificant.

Due to constraints in tank size and the geometry of the experimental setup, there was no measurement available to directly assess the scattering contribution from the squid pen in the dorsal-ventral plane, which is of more interest to fisheries applications with downward-looking echo sounders. The pen is a flat, elongated chitinous supporting structure lying internally along the length of the dorsal surface of the mantle. Therefore, if the pen is an important scattering source, its contribution is likely to lead to a large deviation between the tissue-only model predictions and the experimental data at normal incidence in the dorsal-ventral plane. However, in the study conducted previously by Jones *et al.* (2009), good agreement was found between the experimental data and the three-dimensional DWBA numerical model predictions for *T. pacificus* in the dorsal-ventral plane particularly at normal incidence. This result appears to suggest that the pen does not contribute significantly to the scattering in the dorsal-ventral plane, at least in the investigated frequency range.

D. Squid size estimation

One of the primary advantages of using broadband signals and pulse compression techniques is the increased spatial resolution of the measurements, which allows dominant scattering mechanisms to be determined as well as the scatterer size to be estimated. In this study, the width of the squid mantle was relatively accurately assessed by measuring the separation between the two main arrivals in the CPO envelope at normal incidence, assuming an internal sound speed. However, there were some discrepancies between the physically-measured width and the acoustically-inferred width based on the experimental data as well as model predictions (Fig. 6). There was also significant variability in the inferred width based on the experimental data [Fig. 6(b)]. This variability is likely a result of the expansion and contraction of the mantle during squid ventilation.

The mean acoustically-inferred width from the experimental data is smaller than any of the model predictions. It is possible that this is a result of the error associated with performing dimensional measurements on dead specimens (obtained after the acoustic measurements were complete). In this case, the maximum mantle width measured from a collapsed mantle cavity of a dead squid is likely wider than the mantle width for the same animal when alive. Recall that the squid shapes used in the models are scaled according to the dimensional measurements of the squid.

The acoustically-inferred widths from the model predictions are also different from the actual width of the model volumes, although only by a small proportion ($<2.67\%$). The inferred width of the analytical DWBA prolate spheroid model (2.92 cm) is slightly smaller than the short axis of the prolate spheroid (3 cm). The inferred width of the three-dimensional DWBA numerical model (2.96 cm using the arms-folded squid shape and 3.04 cm using the arms-splayed squid shape) are also different than the actual average width (3 cm) of the digital squid volume. The variability of the inferred widths is a combined effect of the shape of the scattering object and the shape of the auto-correlation function (width of the mainlobe and height of the sidelobes) of the replica signal used in pulse compression processing. For the analytical DWBA prolate spheroid model, the smaller inferred width is an artifact that resulted from the summation of the sidelobes of the response of one of the water-body interfaces and the mainlobe of the response of the other interface. For the three-dimensional DWBA numerical models, the high degree of internal inhomogeneities in the squid volume (see Jones *et al.*, 2009, Fig. 2) interacts with the sidelobes of the auto-correlations function and smears the peak locations in the CPO envelope (Lee *et al.*, 2010).

E. Squid shape

This study has shown that the shape of the modeled squid may also have to be adjusted to obtain the most accurate scattering predictions. In this study, the squid shape used in the three-dimensional DWBA numerical model was based on SCT images of different individuals than those used in the actual scattering measurements. Better agreement may have been achieved by using the same individuals for the scattering measurements and the SCT scans. The results of this study also show that the most accurate model predictions are achieved by using squid shapes that do not include the fins and have loosely-folded arms, most closely resembling the observed shape of the squid during the actual experiment (Fig. 8). In a natural environment, squid usually swim with their arms fully folded and the fins fully extended. The splayed arms are only observed during fighting, defense, or reproduction (Hanlon and Messenger, 1998; Hanlon *et al.*, 1999). Therefore, for acoustic data collected in the field,

model predictions made using squid shapes with folded arms and symmetric fins may produce the best agreement with the data.

F. Modeling squid aggregations

Depending on the species, squid in their natural environment may be found dispersed or in aggregations. To accurately model the scattering from squid aggregations, care must be taken to select the shape of individual squid in the aggregation, the distribution of the squid angle of orientation relative to the sonar beam, as well as the distribution of squid size.

For data collected using downward-looking sonar beams, the shape of the fins is particularly important when the angle of orientation is dominated by near-normal angles (Fig. 9). In field applications, the three-dimensional DWBA numerical model using squid shapes with fins fully extended is likely to give the best modeling results (see Sec. V E). However, errors in the estimates of the angle-of-orientation and size distributions may result in larger errors in the estimated biomass than the choice of different squid shapes (Lawson *et al*., 2006). The angle-of-orientation distribution of the squid relative to the sonar beam can also dictate the choice of models. For example, when the angle of orientation is dominated by near-normal angles, all models, including the analytical DWBA prolate spheroid model, give similar results for averaged TS. However, when the angle of orientation is dominated by off-normal angles, the three-dimensional DWBA numerical model is necessary to accurately predict averaged TS, and the analytical DWBA prolate spheroid model is likely to under-predict the averaged TS in this case.

VI. SUMMARY AND CONCLUSIONS

This study presents a set of controlled laboratory measurements of broadband acoustic scattering from live squid at all angles of orientation in the lateral plane. The results indicate that sophisticated models are necessary to predict the scattering over a wide range of important conditions.

The performance of two DWBA-based models, a closed-form analytical prolate spheroid model and a three-dimensional numerical model, have been compared to the data. By using the three-dimensional DWBA numerical model and digitally manipulating the squid shape, it was possible to assess the scattering contributions from individual body parts, such as the fins and the arms. It has been found that the analytical DWBA prolate spheroid model can accurately predict the measured TS over a narrow range of angles of orientation near normal incidence, while the three-dimensional DWBA numerical model can predict the measured TS across a wider range of angle of orientation. Results of the data-model comparison also show that (1) both DWBA-based models are capable of explaining the observed dominant scattering features at normal incidence, but only the three-dimensional DWBA numerical model can explain the dominant scattering features at angles of orientation well away from normal incidence, (2) the contributions from the front and back interfaces of the squid dominate the scattering at normal incidence, while the arms have a significant effect at other angles, and (3) the scattering from the squid appears to be dominated by the fluid-like weak scattering properties of squid.

One of the ultimate goals of this study is to improve the acoustically-inferred estimates of the distribution and abundance of squid in the ocean. For squid species commonly found in aggregations, potential field applications for the downward-looking sonar and the side-looking sectors in the multibeam systems were investigated by comparing the measured TS to the TS predictions, both averaged over several angle-of-orientation distributions. It has been found that the analytical DWBA prolate spheroid model can only predict the averaged TS for angle-of-orientation distributions dominated by near-normal angles, while the three-dimensional DWBA numerical model was able to reproduce the observed averaged TS except for a small subset of the data collected at near end-on incidence. The incorporation of precise modeling parameters in the three-dimensional DWBA numerical model, including an accurate representation of the squid shape, squid muscle material properties, as well as appropriate estimation of the angle-of-orientation and size distributions, are required to improve the accuracy of the TS estimates.

Finally, squids are a diverse group of animals with a wide range of sizes and shapes, but general anatomical features for these animals are similar for most species. Therefore, the understanding developed in this study through measurements and modeling of the scattering from *L. pealeii* may be applied to guide the modeling for other squid species.

ACKNOWLEDGMENTS

The authors would like to thank Benjamin Jones in the Naval Postgraduate School for providing the computer program for the three-dimensional DWBA numerical model and comments on the manuscript. We thank Dr. Roger Hanlon at the Marine Biological Laboratory (MBL) for providing information on the life history and behavior of squid, Dr. Aran Mooney at the Woods Hole Oceanographic Institution (WHOI) and Justine Allen at MBL for their assistance and suggestions on the sedation and handling of squid, and Dr. Michael Jech at the Northeast Fisheries Science Center for suggestions on the experimental setup. We also thank Ed Enos at MBL for providing live squid and Keenan Ball at WHOI for providing the linear power amplifier. Funding for this research was provided by the Taiwan Merit Scholarship (NSC-095-SAF-I-564-021-TMS) and the Academic Program Office at WHOI.

APPENDIX A: BACKGROUND REVERBERATION, DATA QUALITY, AND NOISE ADDITION

A threshold background noise level was established to determine the data quality for the acoustic measurements. This frequency-dependent background noise threshold [Fig. 10(a)] was obtained by taking the median value of the 200 pings of background reverberation on a frequency-by-

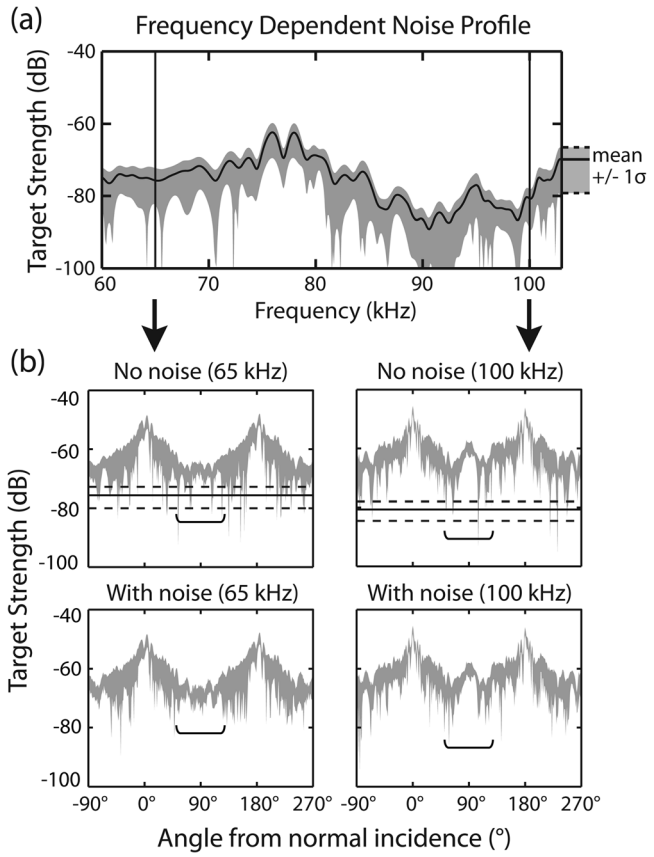

FIG. 10. Noise addition procedure for model predictions. (a) The frequency dependent background noise profile (including reverberation) across the usable band of the experiment. (b) TS predictions with noise added (top row) and without noise added (bottom row) based on the three-dimensional DWBA numerical model. The solid line is the mean of the measured or added noise. The gray or white area between the two dashed lines indicates the range between ±1 standard deviation from the mean. The brackets indicate regions where the effect of noise addition is more prominent. Model predictions below the noise threshold were omitted.

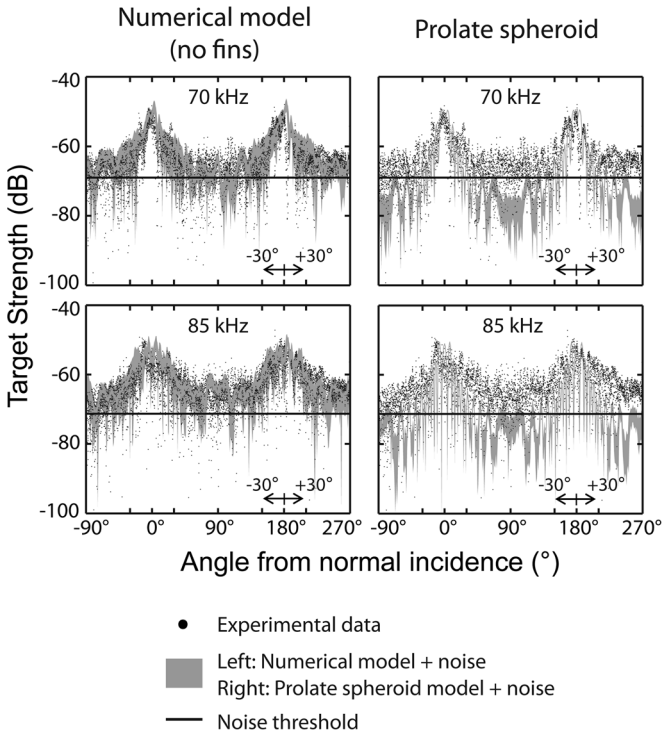

FIG. 11. Comparison of the performance of the three-dimensional DWBA numerical model and the analytical DWBA prolate spheroid model at two frequencies. Frequency-dependent noise was added to both models to enable valid comparison with the data. Dots represent the ping-by-ping experimental data. The gray area indicates the range of ±1 standard deviation from the mean of the models. Note that the experimental data and model predictions lower than the background noise threshold (black lines) were not omitted to illustrate the difference clearly.

frequency basis. A SNR of 6 dB was imposed to control the data quality: all TS values smaller than 6 dB above the threshold was considered unacceptably noisy and discarded. TS measurements within the frequency range of 71.5–82 kHz were also discarded, because this frequency band was observed to be constantly noisy. The SNR in this band was especially low at off-normal angles of orientation.

Since noise from various sources is contained in the experimental data and all model predictions are essentially "noise-free," noise was added to the model prediction to achieve valid data-model comparison [Fig. 10(b)]. First, the mean and standard deviation of the absolute values of the real and imaginary part of the scattering amplitude for the background reverberations were calculated. Normally-distributed random numbers using the above statistical values were then generated independently to construct the real and imaginary parts of the noise. The final noise-added model predictions were produced by coherently adding the noise-free model predictions and the complex noise

$$f_{bs,mn} = f_{bs,m} + f_{bs,n}, \tag{A1}$$

where $f_{bs,mn}$ and $f_{bs,m}$ are the model backscattering amplitude with and without noise added, respectively, and $f_{bs,n}$ is the generated complex noise. The effect of the noise addition is more prominent at angles away from normal incidence with lower predicted TS [indicated by the brackets in Fig. 10(b)].

APPENDIX B: PERFORMANCE OF THE ANALYTICAL DWBA PROLATE SPHEROID MODEL

To investigate the performance of the analytical DWBA prolate spheroid model, noise was added to the model predictions following the same procedure described in Appendix A. The performance of this simple model is compared to that of the three-dimensional DWBA numerical model in Fig. 11. The prolate spheroid model predictions significantly underestimate the TS at angles roughly >30° on both sides of normal incidence, but the three-dimensional DWBA numerical model generally follows the distribution of the experimental data across all angles of orientation.

Arnaya, I. N., and Sano, N. (**1990**). "Studies on acoustic target strength of squid VI. Simulation of squid target strength by prolate spheroid model," Bull. Fac. Fish. Hokkaido Univ. **41**, 32–42.

Arnaya, I. N., Sano, N., and Iida, K. (**1989**). "Studies on acoustic target strength of squid II. Effect of behaviour on averaged dorsal aspect target strength," Bull. Fac. Fish. Hokkaido Univ. **40**, 83–99.

Au, W. W. L., and Benoit-Bird, K. J. (**2008**). "Broadband backscatter from individual Hawaiian mesopelagic boundary community animals with

implications for spinner dolphin foraging," J. Acoust. Soc. Am. **123**, 2884–2894.
Benoit-Bird, K. J., Gilly, W. F., Au, W. W. L., and Mate, B. (**2008**). "Controlled and in situ target strengths of the jumbo squid *Dosidicus gigas* and identification of potential acoustic scattering sources," J. Acoust. Soc. Am. **123**, 1318–1328.
Boyle, P. R., and Rodhouse, P. (**2005**). *Cephalopods: Ecology and Fisheries* (Wiley-Blackwell, Oxford), pp. 259–298.
Chu, D., Foote, K. G., and Stanton, T. K. (**1993**). "Further analysis of target strength measurements of Antarctic krill at 38 and 120 kHz: Comparison with deformed cylinder model and inference of orientation distribution," J. Acoust. Soc. Am. **93**, 2985–2988.
Chu, D., and Stanton, T. K. (**1998**). "Application of pulse compression techniques to broadband acoustic scattering by live individual zooplankton," J. Acoust. Soc. Am. **104**, 39–55.
Chu, D., Wiebe, P., and Copley, N. (**2000**). "Inference of material properties of zooplankton from acoustic and resistivity measurements," ICES J. Mar. Sci. **57**, 1128–1142.
Foote, K. G., Knutsen, T., Atkins, P. R., Bongiovanni, C., Francis, D. T. I., Eriksen, P. K., Larsen, M. T., and Mortensen, T. (**2000**). "Broadband echo spectra from euphausiids and copepods," J. Acoust. Soc. Am. **108**, 2469.
Foote, K. G., Knutsen, T., Atkins, P. R., Bongiovanni, C., Francis, D. T. I., Eriksen, P. K., and Mortensen, T. (**1999**). "A seven-octave-bandwidth echo sounding system for application to fish and zooplankton," J. Acoust. Soc. Am. **105**, 994.
Goss, C., Middleton, D., and Rodhouse, P. (**2001**). "Investigations of squid stocks using acoustic survey methods," Fish. Res. **54**, 111–121.
Hanlon, R. T., Maxwell, M. R., Shashar, N., Loew, E. R., and Boyle, K. L. (**1999**). "An ethogram of body patterning behavior in the biomedically and commercially valuable squid *Loligo pealei* off Cape Cod, Massachusetts," Biol. Bull. **197**, 49–62.
Hanlon, R. T., and Messenger, J. B. (**1998**). *Cephalopod Behaviour* (Cambridge University Press, New York), pp. 31–131.
Iida, K., Takahashi, R., Tang, Y., Mukai, T., and Sato, M. (**2006**). "Observation of marine animals using underwater acoustic camera," Jpn. J. Appl. Phys., Part 1 **45**, 4875–4881.
Johnson, M. L. (**1993**). "Orientation dependence of the acoustic backscatter for elongated zooplankton," Master's thesis, MIT-WHOI Joint Program, Applied Ocean Science and Engineering, Cambridge, MA.
Jones, B. A. (**2006**). "Acoustic scattering of broadband echolocation signals from prey of blainville's beaked whales: modeling and analysis," Master's thesis, MIT-WHOI Joint Program, Applied Ocean Science and Engineering, Cambridge, MA.
Jones, B. A., Lavery, A. C., and Stanton, T. K. (**2009**). "Use of the distorted wave Born approximation to predict scattering by inhomogeneous objects: Application to squid." J. Acoust. Soc. Am. **125**, 73–88.
Kajiwara, Y., Iida, K., and Kamei, Y. (**1990**). "Measurement of target strength for the flying squid (*Ommastrephes bartrami*)," Bull. Fac. Fish. Hokkaido Univ. **41**, 205–212.
Kang, D., Iida, K., Mukai, T., and Kim, J. (**2006**). "Density and sound speed contrasts of the japanese common squid *Todarodes pacificus* and their influence on acoustic target strength," Fish. Sci. **72**, 728–736.
Kang, D., Mukai, T., Iida, K., Hwang, D., and Myoung, J. (**2005**). "The influence of tilt angle on the acoustic target strength of the Japanese common squid (*Todarodes pacificus*)," ICES J. Mar. Sci. **62**, 779–789.
Kawabata, A. (**1999**). "Measurement of the target strength of Japanese flying squid, *Todarodes pacificus Steenstrup*," Bull. Tohoku Reg. Fish. Res. Lab. 29–40.
Kawabata, A. (**2001**). "Measurement of the target strength of live squid, *Todarodes pacificus Steenstrup,* in controlled body tilt angle." Bull. Tohoku Reg. Fish. Res. Lab. 61–67.
Kawabata, A. (**2005**). "Target strength measurements of suspended live ommastrephid squid, *Todarodes pacificus,* and its application in density estimations," Fish. Sci. **71**, 63–72.
Lange, A. M. T., and Johnson, K. L. (**1981**). "Dorsal mantle length-total weight relationships of squids *Loligo pealei* and *Illex illecebrosus* from the Atlantic coast of the united states," NOAA Technical Report NMFS SSRF-745.
Lavery, A. C., Chu, D., and Moum, J. N. (**2010**). "Measurements of acoustic scattering from zooplankton and oceanic microstructure using a broadband echosounder," ICES J. Mar. Sci. **67**, 379–394.
Lavery, A. C., and Ross, T. (**2007**). "Acoustic scattering from double-diffusive microstructure," J. Acoust. Soc. Am. **122**, 1449–1462.
Lavery, A. C., Stanton, T. K., McGehee, D. E., and Chu, D. (**2002**). "Three-dimensional modeling of acoustic backscattering from fluid-like zooplankton," J. Acoust. Soc. Am. **111**, 1197–1210.
Lawson, G. L., Wiebe, P. H., Ashjian, C. J., Chu, D., and Stanton, T. K. (**2006**). "Improved parameterization of antarctic krill target strength models," J. Acoust. Soc. Am. **119**, 232–242.
Lee, W. J., Lavery, A. C., and Stanton, T. K. (**2010**). "Interpretation of the compressed pulse output for broadband acoustic scattering from inhomogeneous weakly scattering objects," J. Acoust. Soc. Am. **128**, 2460.
Madsen, P. T., Wilson, M., Johnson, M., Hanlon, R. T., Bocconcelli, A., de Soto, N. A., and Tyack, P. L. (**2007**). "Clicking for calamari: toothed whales can echolocate squid *Loligo pealeii*," Aquat. Biol. **1**, 141–150.
Medwin, H., and Clay, C. S. (**1998**). *Fundamentals of Acoustical Oceanography* (Academic Press, San Diego, CA), pp. 348–401.
Mooney, T. A., Lee, W.-J., and Hanlon, R. T. (**2010**). "Long-duration anesthetization of squid (*Doryteuthis pealeii*)," Mar. Freshwater Behav. Physiol. **43**, 297–303.
Morse, P. M., and Ingard, K. U. (**1987**). *Theoretical Acoustics* (Princeton University Press, Princeton, NJ), pp. 400–466.
Mukai, T., Iida, K., Sakaguchi, K., and Abe, K. (**2000**). "Estimations of squid target strength using a small cage and theoretical scattering models," in *Proceedings of the JSPS-DGHE International Symposium Fisheries Science in Tropical Area*, pp. 135–140.
O'Dor, R. (**2002**). "Telemetered cephalopod energetics: swimming, soaring, and climbing," Integr. Comp. Biol. **42**, 1065–1070.
Payne, A. G., Agnew, D. J., and Pierce, G. J. (**2006**). "Trends and assessment of cephalopod fisheries" Fish. Res. **78**, 1-3.
Reeder, D. B., Jech, J. M., and Stanton, T. K. (**2004**). "Broadband acoustic backscatter and high-resolution morphology of fish: Measurement and modeling," J. Acoust. Soc. Am. **116**, 747–761.
Rodhouse, P. G. (**2001**). "Managing and forecasting squid fisheries in variable environments," Fish. Res. **54**, 3–8.
Roper, C. F. E., Sweeney, M. J., and Nauen, C. E. (**1984**). *Cephalopods of the World: An Annotated and Illustrated Catalogue of Species of Interest to Fisheries* (United Nations Development Programme, Rome), pp. 5, 97–98.
Santos, M. B., Clarke, M. R., and Pierce, G. J. (**2001**). "Assessing the importance of cephalopods in the diets of marine mammals and other top predators: problems and solutions," Fish. Res. **52**, 121–139.
Seibel, B. A., Goffredi, S. K., Thuesen, E. V., Childress, J. J., and Robison, B. H. (**2004**). "Ammonium content and buoyancy in midwater cephalopods," J. Exp. Mar. Biol. Eco. **313**, 375–387.
Stanton, T. K. (**2009**). "Broadband acoustic sensing of the ocean," J. Mar. Acoust. Soc. Jpn. **36**, 19–31.
Stanton, T. K., and Chu, D. (**2000**). "Review and recommendations for the modeling of acoustic scattering by fluid-like elongated zooplankton: euphausiids and copepods," ICES J. Mar. Sci. **57**, 793–807.
Stanton, T. K., and Chu, D. (**2004**). "On the acoustic diffraction by the edges of benthic shells," J. Acoust. Soc. Am. **116**, 239–244.
Stanton, T. K., Chu, D., Jech, J. M., and Irish, J. D. (**2010**). "New broadband methods for resonance classification and high-resolution imagery of fish with swimbladders using a modified commercial broadband echosounder," ICES J. Mar. Sci. **67**, 365–378.
Stanton, T. K., Chu, D., and Wiebe, P. H. (**1998a**). "Sound scattering by several zooplankton groups. II. Scattering models," J. Acoust. Soc. Am. **103**, 236–253.
Stanton, T. K., Chu, D., Wiebe, P. H., and Clay, C. S. (**1993**). "Average echoes from randomly oriented random-length finite cylinders: Zooplankton models," J. Acoust. Soc. Am. **94**, 3463–3472.
Stanton, T. K., Chu, D., Wiebe, P. H., Eastwood, R. L., and Warren, J. D. (**2000**). "Acoustic scattering by benthic and planktonic shelled animals," J. Acoust. Soc. Am. **108**, 535–550.
Stanton, T. K., Chu, D., Wiebe, P. H., Martin, L. V., and Eastwood, R. L. (**1998b**). "Sound scattering by several zooplankton groups. I. Experimental determination of dominant scattering mechanisms," J. Acoust. Soc. Am. **103**, 225–235.
Starr, R., Thorne, R., Rodhouse, P., Dawe, E., and O'Dor, R. (**1998**). "Acoustic assessment of squid stocks," in *Squid Recruitment Dynamics* (FAO Fish. Tech. Pap. No. 376, Rome), pp. 181–198.